Introduction to mass transfer in single-use bioreactors

Introduction

Mass transfer in Thermo Scientific™ HyPerforma™ Single-Use Bioreactors (S.U.B.s) is critical to the growth of cells in culture, yet is often a misunderstood principle due to its complexity. A basic understanding of mass transfer and its underlying principles is essential to single-use bioreactor design, determining bioreactor operating parameters, and optimizing culture conditions. This paper aims to elucidate the standard mass transfer model, and details how the application of critical mass transfer principles to the design and operation of the HyPerforma S.U.B. helps to achieve optimal mass transfer performance for cell culture operations.

Stirred bioreactor background

Bioreactor design, operation, and scalability (bench to large-scale production) criteria are dependent on multiple factors, including reactor geometry, agitator selection, power input, mixing, agitator shear, critical control parameter sensing, sparging, and bubble shear. Virtually all of these factors also play a role in the efficiency of the reactor, including oxygen mass transfer. The essential nature of oxygen mass transfer as a potential growth-limiting factor in stirred bioreactor systems makes it critical for the engineer to both understand and optimize.

Gas mass transfer into the liquid phase in stirred bioreactors is usually achieved through either super-surface (i.e., headspace sweep or overlay) or sub-surface (i.e., sparging) aeration using a combination of gases that includes air, N_2, CO_2, and O_2. Sparging traditionally provides most of the mass transfer, and is performed by spargers that typically sit below the agitator to maximize the entrainment of bubbles in the mixing patterns of the reactor. Selection criteria of sparger types vary widely depending on desired performance and customer requirements.

Stirred-tank bioreactors were originally based on the design principles of traditional microbial fermentors, which relied heavily on stainless steel technologies. As such, the design of most sparge systems found in stirred-tank bioreactors was not intended for mammalian cell cultures. Typical microbial fermentors rely on high-shear mixers, such as Rushton impellers, to break up bubbles formed in less efficient sparger designs. Coupled with high gas flow rates, this results in violent gas distribution to provide sufficient mass transfer. While most microbial fermentation cultures (such as *E. coli*) can grow well while being subjected to these conditions, mammalian cell culture usually requires a gentle mixing approach using pitched-blade or marine impellers, and lower gas shear rates, which require differently engineered spargers [1–3]. Thus, for modern cell culture bioreactors, it is critical to carefully engineer spargers in terms of material, pore size and quantity, sparger geometry, location relative to the impeller, effective gas flow range, and resulting operational gas entrance velocity.

Mass transfer background

Mass transfer model

Mass transfer of either O_2 or CO_2 in a gassed bioreactor system can be defined according to the simplified gas-liquid film theory [4] as defined in Equation 1 and depicted in Figure 1:

$$\frac{dC_L}{dt} = k_L a \cdot (C_L^* - C_L) \qquad \text{Equation 1}$$

where C_L is the molecule's concentration in solution, C^*_L is the saturation concentration of the molecule in solution, t is time, and $k_L a$ is defined as the mass transfer coefficient. This equation outlines the flux or movement of a molecule from gaseous to liquid phase (or vice versa) according to gas concentration differences and the inherent resistance of that movement. The ability to interpret and manipulate this equation is essential to maximizing and optimizing O_2 and CO_2 mass transfer in solution.

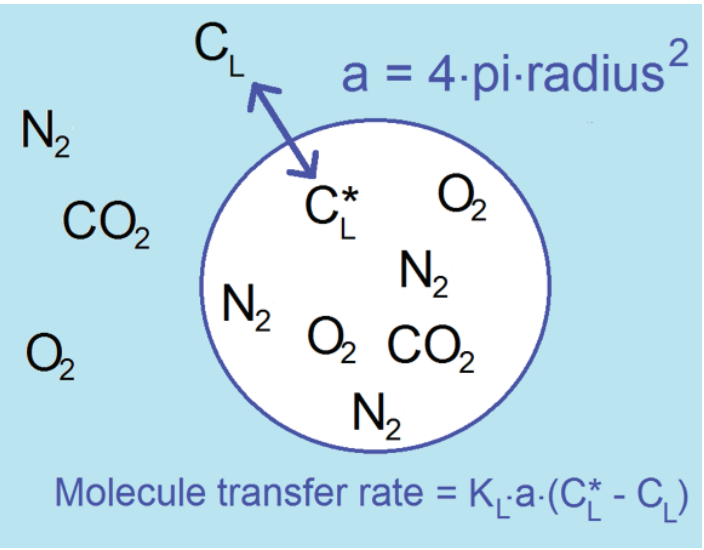

Figure 1. Molecule transfer rate equation description.

The mass transfer coefficient, $k_L a$, is a combination of the resistance to mass transfer across a physical barrier, k_L (mass transfer through the liquid–gas film, similar to heat transfer through a wall), and the area of mass transfer flux, a. Mass transfer resistance is highly dependent on liquid properties and chemistry, including liquid surface tension, ion and nutrient concentration, surfactant concentration, and liquid temperature. The area of transfer is solely dependent on the mean diameter of a single bubble. In practice, however, estimation of the total bubble surface area in a sparged system of millions of bubbles of various sizes is difficult to determine, particularly in systems that rely on bubble breakage for mass transfer. Therefore, these terms are combined into the single mass transfer coefficient, $k_L a$.

The term $(C_L^* - C_L)$ is the difference between the saturation concentration of the sparged gas and the operating concentration in solution. In effect, the difference in gas concentrations or partial pressures provides the driving force to move molecules across the liquid–gas film according to Henry's Law, which is further discussed later. This term can be manipulated by adjusting each parameter to achieve the desired effect. For example, when using pure oxygen, C_L^* for oxygen is approximately five times higher than it is when using air as the primary gas. Similarly, the dissolved oxygen (DO) setpoint can be decreased to increase the driving force.

Measuring mass transfer

Experimentally, Thermo Fisher Scientific measures the effective mass transfer coefficient using the dynamic method [4]. For the $k_L a$ of O_2, this is performed by sparging air into an N_2-saturated solution at a given flow rate and agitation speed. Similarly, for $k_L a$ of CO_2, air is sparged into a CO_2-saturated solution. Integrating Equation 1 yields Equation 2, which shows that $k_L a$ is the slope of the line formed by the concentration gradient over time. An example is depicted in Figure 2 showing the raw DO data and the processed data, which are used to calculate a $k_L a$ of 12.0/hr.

$$k_L a = \frac{\ln\left(\frac{C_L^* - C_{L1}}{C_L^* - C_{L2}}\right)}{t_2 - t_1} \qquad \text{Equation 2}$$

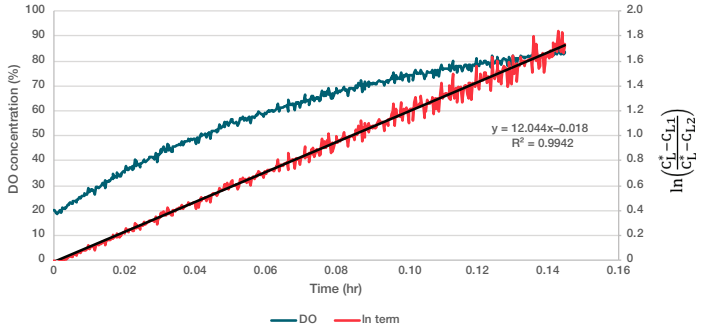

Figure 2. Example data for $k_L a$ determination.

The standard test solution used at Thermo Fisher Scientific is composed of 1 g/L of poloxamer 188 and 3.5 g/L of HEPES. The solution is heated to 37°C and titrated to pH 7.25 at air saturation (CO_2 desaturation). This test solution is chosen specifically to mimic typical mammalian cell culture media for reasons that will be discussed hereafter.

Because the mass transfer coefficient is a system-dependent variable, when characterizing a S.U.B. system, operating parameters including agitation rate and gas flow rates through specific spargers are adjusted per test condition to produce a map of k_La values.

Other factors that affect k_La include:

- Molecule solubility: dependent on temperature, pressure, and solution compounds
- Bubble surface area and residence time: bubble size, gas flow rate, agitation, and sparger position
- Concentration gradients: dispersion effects due to sparge size, agitation, and bubble size
- System parameter accuracy: mass flow controllers and agitator
- Probe response times
- Purity of the sparging gases

A change to any one of these variables can affect overall performance of the system, which can complicate comparison, modeling, and eventually scalability of one bioreactor to another.

Effects of gas partial pressures

An important factor in mass transfer is Henry's Law, which states that molecules move according to concentration gradients as determined by gas partial pressure or vapor pressure. Table 1 displays the difference in driving force for O_2 and CO_2 gases during a cell culture process. For example, in a typical cell culture process with a DO setpoint of 30% air saturation when sparging air, the partial pressure difference between gas bubble and liquid is 0.15, whereas when sparging O_2 the difference increases to 0.94. This highlights the effect of the mass transfer equation and how parameters can be manipulated to achieve substantially higher flux rates in practice.

While CO_2 is far more soluble and diffuses at about 10x the rate of O_2 in cell culture, the driving force to remove CO_2 from solution is typically far less than that of adding O_2. Therefore, it can be more difficult to remove sufficient CO_2 from solution, which can lead to CO_2 buildup in culture. Further complicating CO_2 control, CO_2 can dissolve into solution and exist either as $CO_2(aq)$, carbonic acid (H_2CO_3), or bicarbonate (HCO_3^-), as seen in Equation 3. Therefore, if $CO_2(aq)$ concentration and, consequently, carbonic acid concentration are high, bicarbonate anion concentration will also increase, leading to acidification of the system. Because of the slow reaction kinetics of bicarbonate anion to carbonic acid, it is also much more difficult to strip all $CO_2(aq)$ out of a solution.

$$CO_2(g) \leftrightarrow CO_2(aq) + H_2O(l) \leftrightarrow H_2CO_3(aq) \leftrightarrow HCO_3^-(aq) + H^+(aq)$$

Equation 3

Table 1. Driving partial pressure differences available to add O_2 and remove CO_2 in typical animal cell culture bioreactors (in atm assuming 1 atm ambient pressure) and corresponding mass ratios of dissolved gases.

Reactor dissolved O_2 setpoint	CO_2 stripping partial pressure delta with air or O_2	O_2 delivery partial pressure delta		Mass ratio dissolved gas	
		Sparging with air	Sparging with O_2	CO_2	O_2
30% air saturation	0.06	0.15	0.94	14.4	1
50% air saturation	0.06	0.11	0.89	8.5	1

Bubbles and sparging

Sparger background

In order to generate bubbles of the proper size for cell culture to achieve required levels of O_2 delivery and CO_2 stripping, an understanding of sparger design and function as well as bubble formation is necessary. Spargers employed in stirred-tank bioreactors have traditionally been categorized into two general groups: microspargers and macrospargers. These spargers can be employed either in tandem or as stand-alone units, depending on end result requirements and system capabilities.

Microspargers are usually composed of a sintered material (metal, plastic, or ceramic) that forms a tortuous path for the sparging gas to pass through, terminating in a porous surface from which gas bubbles form and are released into the solution (Figure 3). While a "nominal" pore size for these spargers is given for an individual part, in reality the effective pore size and geometry varies according to a standard distribution curve with ill-defined tolerances [5,6]. This results in bubbles of varying size, which in turn results in widely varying mass transfer performance and reduced predictability of critical parameters, such as gas-entrance velocity and bubble coalescence. Bubble formation as a function of pore size, material properties, solution characteristics, and gas flow is discussed later. The potential advantage of these spargers lies in the creation of micro-sized bubbles (≤1 mm diameter), which are efficient at delivering O_2 but generally less efficient at removing dissolved CO_2 from solution.

Macrospargers include both open-pipe and the more standard drilled-hole sparger (DHS). As stated previously, the traditional design of these macrospargers has been reliant on typical stainless steel fermentation applications, which do not translate well to either mammalian cell culture or single-use systems. In stainless steel fermentation systems, macrospargers create large bubbles that are then broken up and dispersed throughout the reactor (power input >100 W/m^3), whereas macrospargers employed in mammalian cell culture (vessels glass, stainless steel, or single-use) generate bubbles that are poorly dispersed by lower power input (<40 W/m^3). As such, macrospargers in mammalian cell culture systems have typically been used to remove dissolved CO_2 from solution due to the associated large bubble size, while a tandem microsparger is used to fine-tune DO concentrations.

Because each cell culture system has differing O_2, CO_2, agitation, and gassing needs, selection of sparging technology differs widely. Thermo Fisher Scientific has traditionally offered a dual-sparge system, which includes a microsparger and macrosparger to allow for varying customer needs with customizable options available. However, new data show that using a DHS-only control option, especially for systems with a 5:1 turndown ratio, is beneficial as an optimized mass transfer system as well as providing better scalability from pilot to commercial manufacturing reactors.

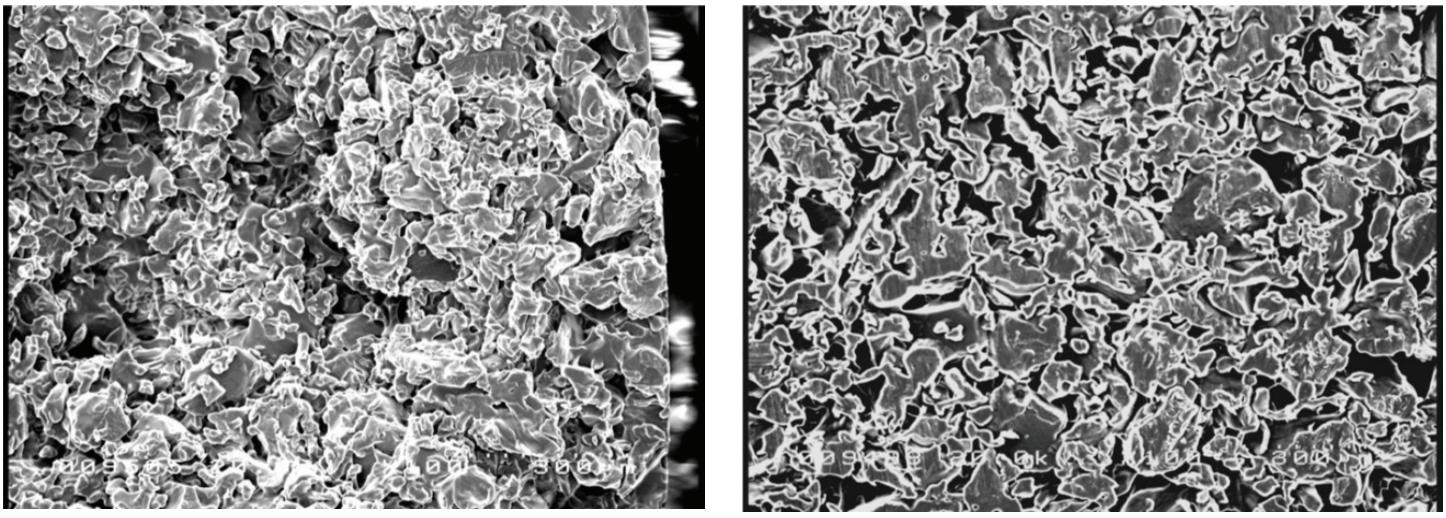

Figure 3. Cross-section (left) and surface (right) scanning electron microscope images of sintered PVDF sparger.

Bubble formation and bubble sizes

Bubble formation at the sparger surface plays a considerable role in mass transfer performance, and must be understood to properly design microspargers and macrospargers. Extensive studies outline the effects of multiple parameters on bubble formation, final bubble size, and rise velocity, including material surface, solution, and gas properties [7–9]. These will be discussed briefly here to demonstrate that optimal sparger design and operating parameters are critical, and often do not correlate well between stainless steel and single-use systems.

Bubbles are formed at sparger pores when gas is forced through a pore and into a solution. Various forces act on the bubble, determining the resultant bubble size. Essentially, there is a balance of upward and downward forces dependent on pore diameter, liquid and gas density, gas and bubble rise velocities, liquid surface tension, material surface energy, and liquid viscosity [7–10]. Additionally, hydrostatic pressure as experienced in low-pressure single-use bioreactors [8,11] and liquid flow across the sparger surface [12] can affect final bubble size. When upward forces are larger than downward forces, a bubble is formed and rises through the liquid, transferring gas according to the standard mass transfer equation. Some of these forces are shown in Figure 4, with descriptions of the forces provided in Table 2.

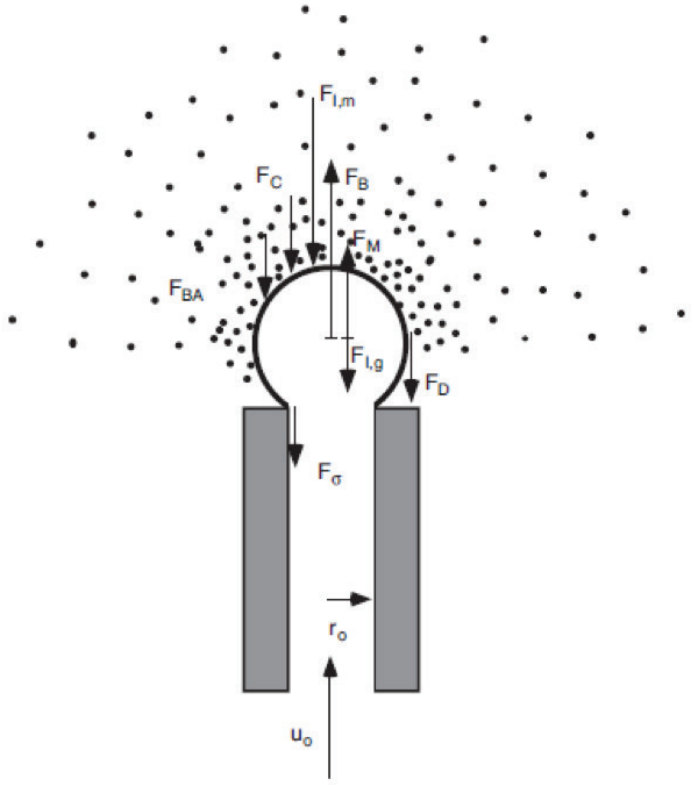

Figure 4. The balance of forces acting on a growing bubble [7].

Table 2. Forces acting during the bubble formation process [9].

Force	Description	Main factors	Equation
F_B	Buoyancy	Bubble diameter, liquid/gas density difference	$\frac{\pi}{6} d_b^3 (\rho_l - \rho_g) g$
F_M	Gas momentum	Orifice diameter, gas density, gas velocity	$\frac{\pi}{4} D_o^2 \rho_g u_o^2$
F_D	Liquid drag	Drag force, bubble diameter, liquid density, bubble velocity	$C_D \left(\frac{\pi}{4} d_b^2\right) \frac{\rho_l u_b^2}{2}$
F_σ	Surface tension	Orifice diameter, liquid surface tension, solid surface energy	$\pi D_o \sigma_l \cos\gamma$
$F_{I,g}$	Bubble inertia	Gas density, bubble diameter, bubble velocity	$\frac{d}{dt}\left[\rho_g \left(\frac{\pi}{6} d_b^3\right) u_b\right]$
F_C	Particle-bubble collision	Orifice diameter, solids hold-up, solids density, bubble expansion velocity	$\frac{\pi}{4} D_o^2 (1-e) \varepsilon_s \rho_s u_e^2$
$F_{I,m}$	Suspension inertia	Liquid density, suspension velocity, bubble volume change	$\frac{d(\iiint \rho_m u_m \delta V)}{dt}$

For smaller bubbles (<1 mm diameter), which are generally spherical, the viscous and surface tension forces dominate bubble formation. This is especially noticeable in bubbles generated by spargers of different material types or solutions of different chemistry. For intermediate-sized bubbles (1–4 mm diameter), surface tension and buoyancy forces are most important in determining how bubbles change in shape and move within a liquid. For larger bubbles (>4 mm diameter) inertial forces dominate, and other forces, such as surface energy, surface tension, and viscosity, are essentially negligible. This leads to amorphous geometries and more frequent bubble collapse or coalescence.

The impact of material construction on bubble size is seen in Figure 5, which compares the bubble sizes of sintered spargers of stainless steel (SS), polyvinylidene difluoride (PVDF), and polyethylene (PE) of similar pore size but varying surface energy. Stainless steel is a very high–surface energy material (>700 mN/m) compared to the low surface energies of PVDF (30 mN/m) and PE (35 mN/m). This means that water prefers to be in contact with stainless steel, but is repelled by most polymers. In practice, this results in pores on stainless steel spargers creating much smaller bubbles than similar pore sizes on polymer spargers.

As pore size increases, surface energy plays less of a role in bubble formation as seen in Figure 6, which compares bubble sizes from DHSs made of SS and PE. Figures 5 and 6 highlight the definite tipping point in pore size where surface energy ultimately governs the bubble formation and effective mass transfer.

At very large pore sizes, such as those in open-pipe spargers, inertial forces generally dominate bubble formation. Surface properties play a much smaller role, except at very low flow rates [8]. This results in a complex dynamic of bubble formation culminating in larger bubbles that break and coalesce, forming both very large and very small bubbles as seen in Figure 7. As one large bubble exits the sparger at a high flow rate, the momentum of that bubble causes it to mushroom upward. This creates a low-pressure zone below that bubble, which allows a subsequent bubble to elongate to fill that zone. The associated momentum of that bubble causes it to quickly mushroom, which leads to cavitation at the tail end of the bubble, forming microbubbles in its wake.

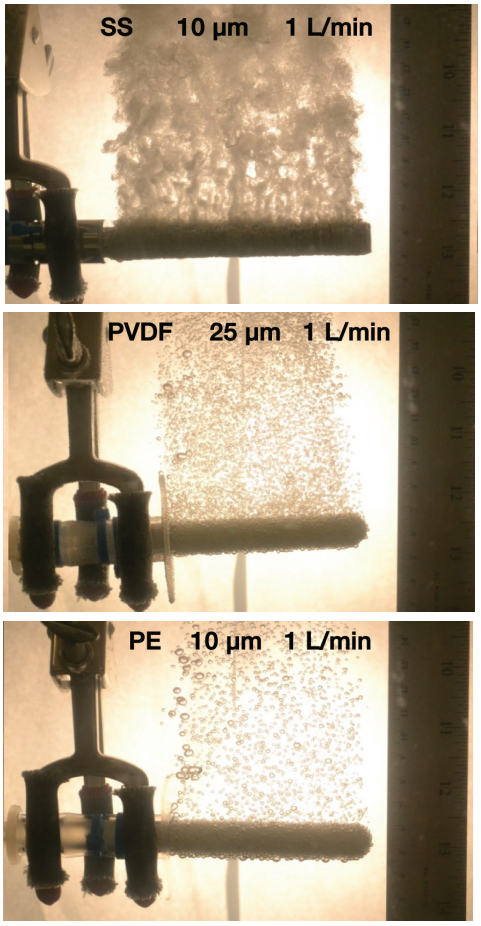

Figure 5. Microspargers made of SS, PVDF, and PE with associated nominal pore sizes sparged with air at 1 L/min into 1 g/L poloxamer 188 solution.

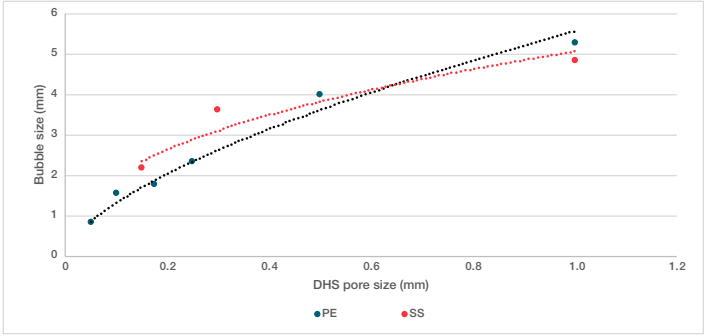

Figure 6. Bubble sizes with respect to pore size for PE and SS spargers.

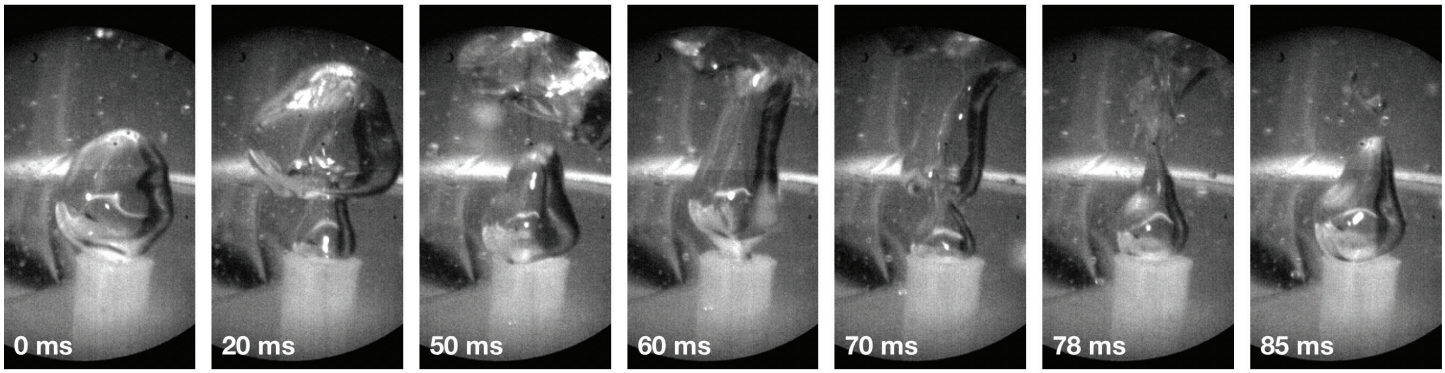

Figure 7. Bubble formation from a 250 L open pipe sparger at 5 slpm air flow and at various time points, as seen with a high-speed camera.

Pore size distribution also plays a large role in bubble formation, especially in microspargers, where there is typically a wide bell curve of effective pore sizes. Gas will flow through the path of least resistance as governed by Equation 4, where ΔP is the capillary pressure, σ_L is the liquid surface tension, and r_p is the effective pore size [10]. For example, gas will flow through larger pores at low gas flow rates (lower pressure), and smaller pores as gas flow rate increases. In systems with higher pore size consistency, such as a well-designed DHS, bubbles will form more evenly across a surface, resulting in more consistent bubble sizes.

$$\Delta P = \frac{2\sigma_L}{r_p} \qquad \text{Equation 4}$$

Equation 4 and the surface tension equation in Table 2 highlight the role liquid surface tension plays in bubble formation. As surface tension decreases, bubbles are not held as strongly to the pore, thus releasing sooner, creating smaller bubbles. This effect is often overlooked. Current DECHEMA guidelines [13] suggest normalizing all k_La testing using water and salt solutions, which have fairly high liquid surface tensions (60–70 mN/m), whereas most cell culture solutions have a far lower surface tension (<40 mN/m). Therefore, using water or water/salt as a test solution will provide results that are not representative of solutions containing surfactants such as poloxamer 188, which is included in most cell culture media [6,14].

DHS design

The HyPerforma S.U.B. implements a precision-laser-drilled DHS that offers many benefits, including limited gas entrance velocity, uniform bubble size across gas flow rates, and linear performance scalability. Gas flow rate must not only be considered with respect to simple bubble formation, but must also relate to effective gas entrance velocity (GEV). While few studies on the effect of GEV on cell viability have been performed, it is generally understood that GEV above 30 m/s creates damaging shear, which is detrimental to cell growth and viability [2,15]. As such, spargers should be designed to limit gas entrance velocities within desired flow ranges. The current DHS from Thermo Fisher Scientific was designed with this in mind. Table 3 highlights the DHS design with respect to GEVs; all GEV values at maximum flow rates of 0.1 vessel volume per minute (VVM) are less than half to one third the literature-reported acceptable limits.

Table 3. Forces acting during the bubble formation process [9].

	Pore size (mm)	Pore quantity	Maximum recommended flow rate (L/min)	GEV at 0.1 VVM (m/s)
50 L	0.178	360	5	9.3
100 L	0.178	570	10	11.8
250 L	0.233	760	25	12.9
500 L	0.368	980	50	8.0
1,000 L	0.445	1,180	100	9.1
2,000 L	0.582	1,380	200	9.1

The pores on the DHS from Thermo Fisher Scientifc are precision-drilled with a laser, with spacing designed to limit bubble-to-bubble interactions and coalescence, ensuring bubble size is uniform and consistent through the entire operating range of recommended gas flow rates. Under low-flow conditions, pressure in the sparger disc builds, forcing bubbles to form within the bioreactor. Based on surface interactions and gas pressures, minimal pores will form bubbles and release them into the system. A release of uniformly sized bubbles will relieve the pressure in the sparge disc, and the process will repeat (Figure 8). This gentle, periodic release of bubbles from individual pores is referred to as pulse-modulated sparging. As the gas flow rate increases, more and more pores form bubbles until all pores are utilized. With still higher gas flow rates, the bubbles form and release more quickly, but still generate similarly sized bubbles. The end effect is a linear quantity of bubbles and resulting bubble surface area formed from the sparger with respect to the operating gas flow range, which results in highly predictable, linear k_La performance for each specific sparger selected for each S.U.B.

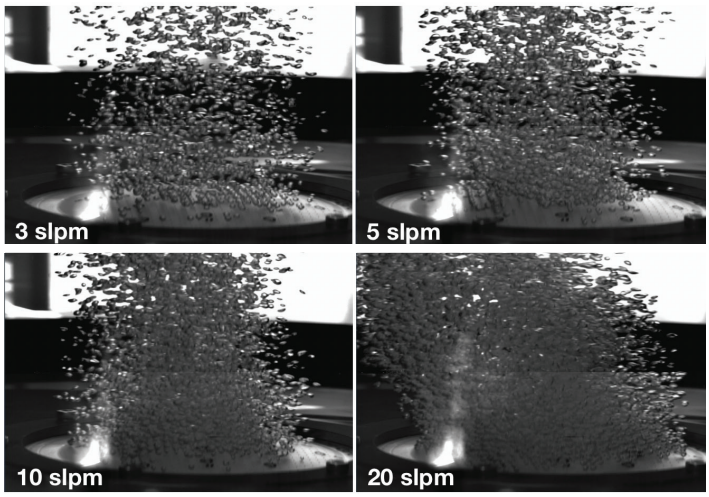

Figure 8. Bubble formation with a 250 L DHS at various gas flow rates.

Mass transfer results

Oxygen mass transfer

Mass transfer for spargers within Thermo Scientific S.U.B.s has been extensively tested within defined operation parameters, as specified in the user's guides and validation guides. The results of the testing show the capabilities and limitations of each sparger for both O_2 and CO_2 mass transfer within the design space of each sparger.

As discussed previously, the DHS shows good scalability across vessel sizes and offers proportional increases in k_La with respect to total gas flow rate (Figure 9), due to the pulse-modulated sparging. Good linear scalability within a vessel allows control systems to proportionally increase associated outputs, such as to an air or O_2 mass flow controller, to support increasing cell densities.

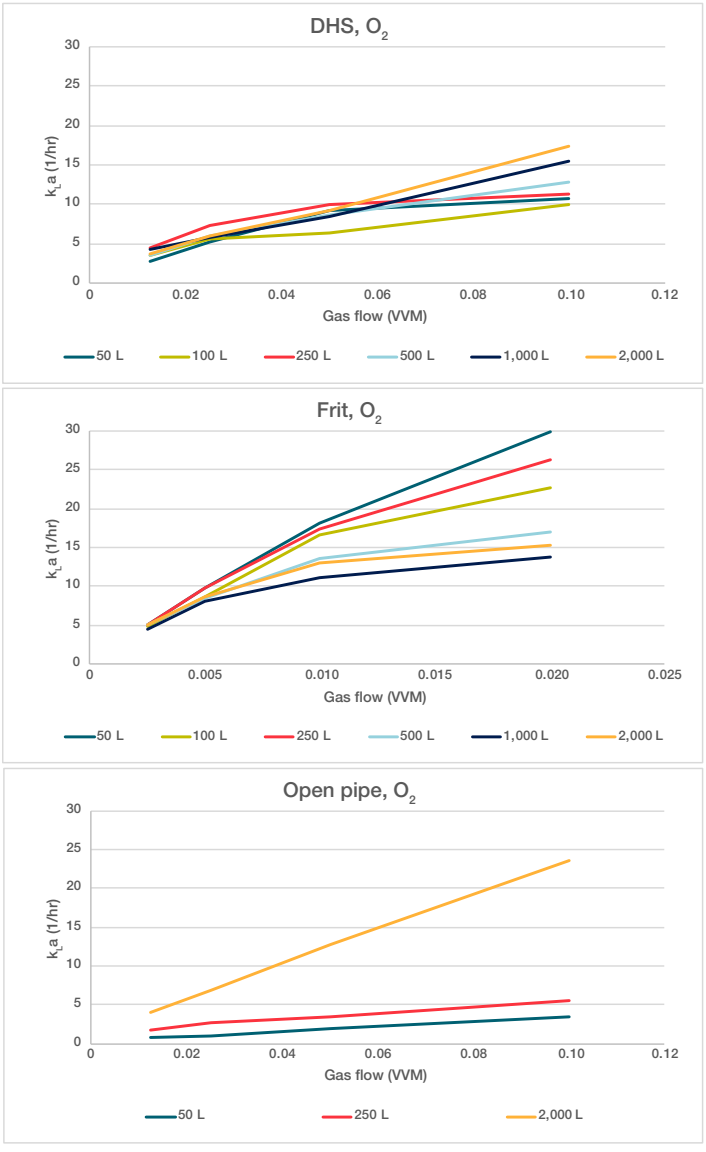

Figure 9. k_La of O_2 in all S.U.B. sizes at various gas flow rates and 30 W/m³ power input for the different spargers.

As opposed to the DHS, the frit sparger exhibits non-linear behavior within specific S.U.B.s and poor scalability across vessel sizes. The frit data in Figure 9 highlight that increasing vessel size and flow rate both lead to diminished performance of the frit. The frit was designed as a single part for use in all systems, and thus is not scaled to each individual S.U.B. size for both surface area and nominal pore size.

As observed, low total flow rate through the frit in the smaller vessels achieves higher k_La than even extreme flow rates in the larger vessels. The observed asymptotic correlation describes the overall effect of microspargers in S.U.B. systems according to principles previously described. At low flow rates, only specific pore sizes are utilized in bubble formation, as described by Equation 4. At increasing flow rates through identical pore sizes, gas momentum and inertial forces start to play a role; while smaller bubbles are now allowed to form, bubbles coming from those and larger pores will also increase in size, ultimately leading to no increase in mass transfer. Additionally, the small bubbles produced by the frit may achieve equilibrium with the surrounding solution, resulting in an inverse relationship between gas flow rate and S.U.B. column height.

The open-pipe sparger exhibits wide mass transfer efficiencies depending on vessel size. This is, in large part, attributed to the effect of gas flow on bubble formation. At a low gas flow rate as tested in the 50 L S.U.B., the bubbles enter very gently, leading to the formation of large bubbles that are very poor at mass transfer. The 250 L S.U.B. begins to enter chaotic bubble formation at increasing flow rates as depicted earlier in Figure 7. This, along with a slightly higher bubble residence time, results in a slight boost in mass transfer. The 2,000 L S.U.B. was ultimately tested at a very high flow rate, leading to highly chaotic bubble formation. The much higher residence time of both the macro- and microbubbles leads to a large boost in O_2 mass transfer.

Carbon dioxide mass transfer

Figure 10 highlights the differences in the effect of each sparger type on CO_2 mass transfer. Both the DHS and frit sparger offer linear scaling within and across vessel sizes, while the open-pipe sparger scales very poorly among tested vessel sizes. The data also highlight the large difference in mass transfer capability of the DHS compared to the frit. While the DHS has larger bubbles, which can pull more CO_2 from solution as the bubbles rise, the frit has much smaller bubbles, which quickly equilibrate with the surrounding solution, leading to poor CO_2 mass transfer despite the higher quantity of bubbles present. Similar to the O_2 mass transfer of the open-pipe sparger, the effects of gas flow on bubble formation greatly impact CO_2 mass transfer.

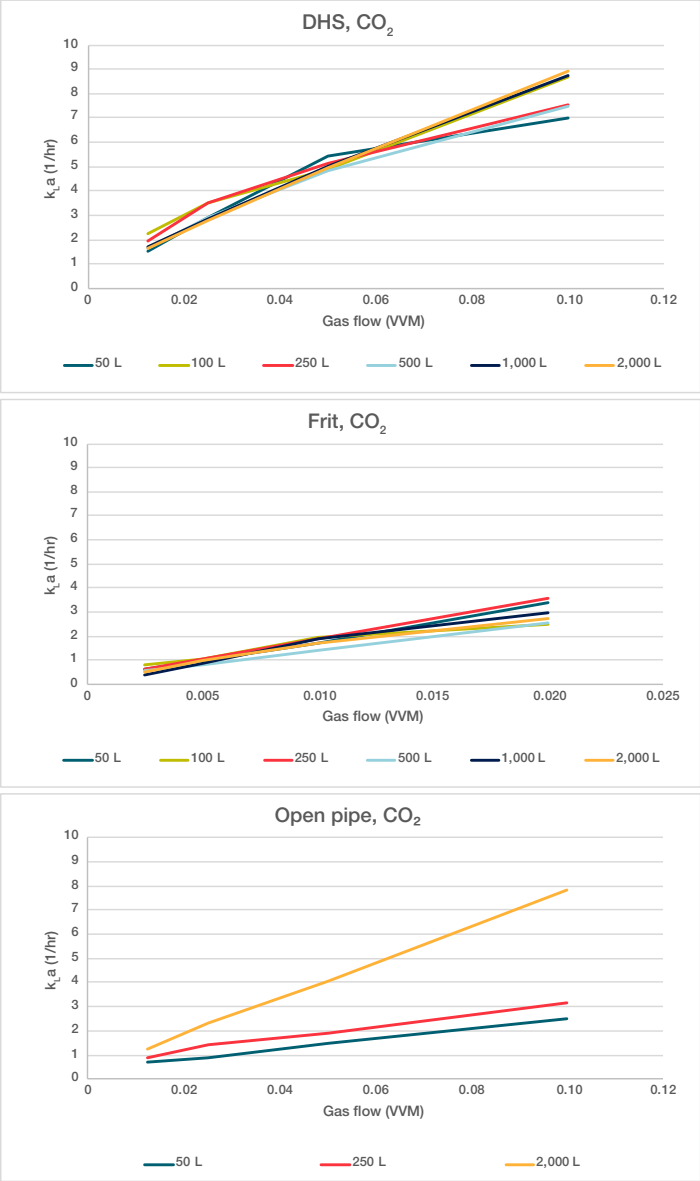

Figure 10. k_La of CO_2 in all S.U.B. sizes at various gas flow rates and 30 W/m³ power input for the different spargers.

This leads to difficulty in scaling among S.U.B. sizes because each open-pipe sparger will yield different results at gas flow rates scaled on a VVM basis.

Mass transfer ratios

While total gas mass transfer is highly important in determining component effectiveness, in practice it is also important to balance both O_2 and CO_2 mass transfer in a bioprocess to ensure proper culture conditions. This has been especially important when scaling to larger-scale reactors and high-density cultures, as sparge systems are generally poorly scaled among systems [13,16,17]. Therefore, it is beneficial to consider the mass transfer ratios of the gases and how they scale between systems.

An important ratio that has been empirically and chemically determined is the respiratory quotient of cell lines (i.e., the rate of CO_2 production relative to the O_2 uptake rate of cells), which is generally close to 1 [18,19]. While this number would suggest it is important to have a CO_2:O_2 k_La ratio (as measured in standard mass transfer experiments) near 1, in actuality the mass transfer coefficient is only a piece of the overall mass transfer flux of a system, as described by Equation 1. Actual molecular transfer is dependent on operating conditions, including DO setpoint and partial pressure of the sparged gas. In practice, when running the DHS with pure oxygen in a variety of cell culture applications in S.U.B.s, a mass transfer ratio of approximately 0.5 has been shown to balance DO and dCO_2 very effectively [20,21].

Figure 11 shows that across all vessel sizes, the DHS remains near a ratio of 0.5 across all tested flow rates. Coupled with the good O_2 mass transfer near 10/hr as seen in Figure 9, this sparger is ideally suited to support a number of culture processes in S.U.B.s. On the other hand, the frit shows a very poor CO_2:O_2 ratio near 0.1–0.2. Using the frit can therefore lead to elevated dCO_2 concentrations and more acidification of the cultures, especially at large scale. The open pipe shows poor scalability among systems, with good ratios at small scale but low ratios at larger scale.

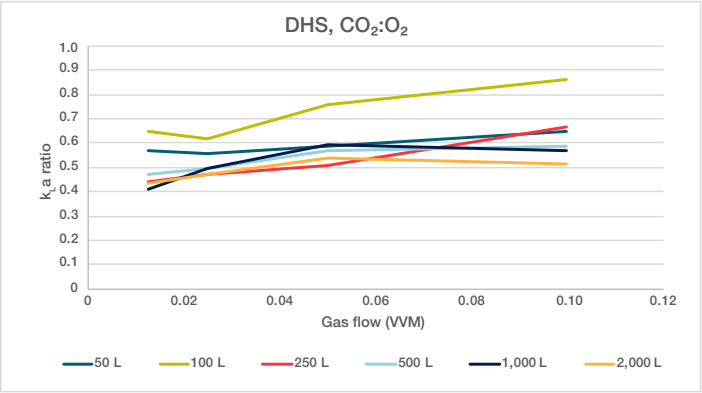

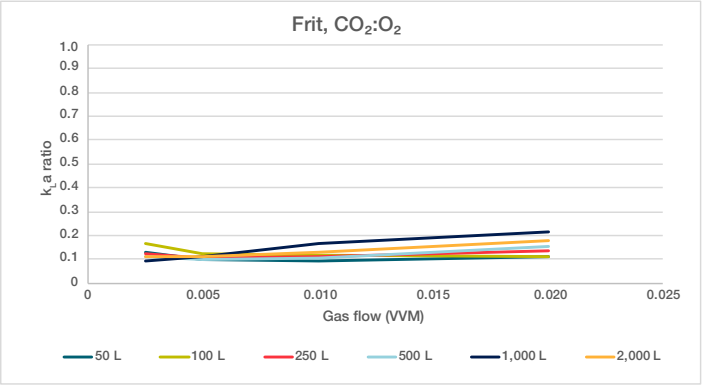

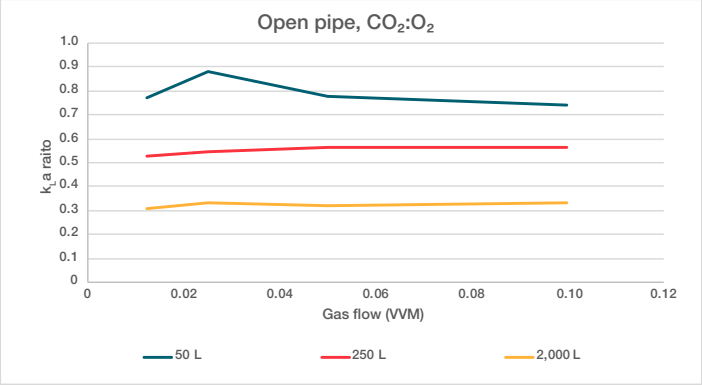

Figure 11. k_La ratios (CO_2:O_2) in all S.U.B. sizes at various gas flow rates and 30 W/m³ power input for the different spargers.

Agitation effects

Agitation also affects bubble dispersion for the different spargers. For the frit, the microbubbles are less buoyant, and therefore are highly dispersed even at low agitation speeds. As agitation increases (i.e., power input per volume increases) further dispersion of the microbubbles does not cause a large increase in mass transfer. Conversely, the DHS creates larger, more buoyant bubbles that are more susceptible to agitation effects. Better bubble distribution at higher agitation rates increases residence time and, therefore, mass transfer coefficients. Similar patterns are seen with CO_2 stripping in similar conditions.

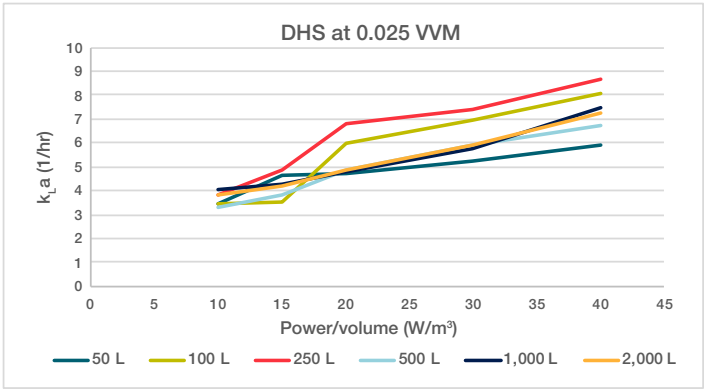

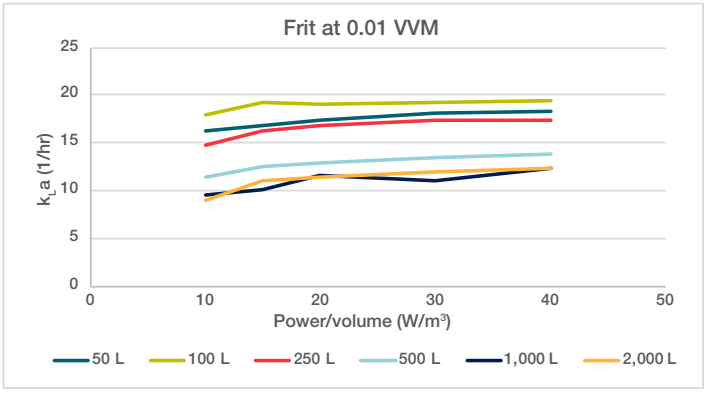

Figure 12. k_La of O_2 in all S.U.B. sizes at various power inputs and specified DHS or frit flow rates.

thermo scientific

Conclusions

This paper has explored the fundamentals of mass transfer to better assist end users of Thermo Scientific S.U.B.s in optimizing their systems. The mathematics of mass transfer, the physics of bubble formation, and the surface interactions leading to the final sparger designs are all pieces essential to better understanding the context of mass transfer results as presented in the S.U.B. validation guides. With the insight presented here, it becomes easier to implement spargers into specifically designed gassing strategies during cell culture operations to achieve optimal results.

References

1. Chisti, Y. (2001) Hydrodynamic damage to animal cells. *Critical Reviews in Biotechnology* 21, 67–110.
2. Hu, W. et al. (2011) The potential of hydrodynamic damage to animal cells of industrial relevance: current understanding. *Cytotechnology* 63, 445–460.
3. Chalmers, J.J. (1994) Cells and bubbles in sparged bioreactors. *Cytotechnology* 15, 311–320.
4. Doran, P.M. (2013) Mass Transfer. In *Bioprocess Engineering Principles* (2nd edn) pp. 416–425, Elsevier.
5. German, R.M. (2010) Thermodynamics of sintering. In *Sintering of Advanced Materials* pp. 3–32, Elsevier.
6. Sieblist, C. et al. (2013) Influence of pluronic F68 on oxygen mass transfer. *Biotechnology Progress* 29, 1278–1288.
7. Luo, X. et al. (1998) Single bubble formation in high pressure liquid—solid suspensions. *Powder Technology* 100, 103–112.
8. Byakova, A.V. et al. (2003) Influence of wetting conditions on bubble formation at orifice in an inviscid liquid. *Colloids and Surfaces A: Physicochemical and Engineering Aspects* 229, 19–32.
9. Yang, G.Q. et al. (2007) Bubble formation and dynamics in gas–liquid–solid fluidization—A review. *Chemical Engineering Science* 62, 2–27.
10. Kazakis, N.A. et al. (2007) Experimental study of bubble formation at porous spargers. Presented at the 6th International Conference on Multiphase Flow, Leipzig, Germany, pp. 1–11.
11. Yoo, D.-H. et al. (1997) Behavior of bubble formation in suspended solution for an elevated pressure system. *Chemical Engineering Science* 52, 3701–3707.
12. Laakkonen, M. et al. (2005) Local bubble size distributions in agitated vessel: comparison of three experimental techniques. *Chemical Engineering Research and Design* 83, 50–58.
13. Meusel, W. et al. (2016) Recommendations for process engineering characterisation of single-use bioreactors and mixing systems by using experimental methods, DECHEMA expert group Single-use Technology.
14. Matsunaga, N. et al. (2009) Estimation of dissolved carbon dioxide stripping in a large bioreactor using model medium. *Journal of Bioscience and Bioengineering* 107, 419–424.
15. Zhu, Y. et al. (2008) NS0 cell damage by high gas velocity sparging in protein-free and cholesterol-free cultures. *Biotechnology and Bioengineering* 101, 751–760.
16. Mostafa, S.S. and Gu, X. (2003) Strategies for improved dCO_2 removal in large-scale fed-batch cultures. *Biotechnology Progress* 19, 45–51.
17. Gray, D.R. et al. (1996) CO_2 in large-scale and high-density CHO cell perfusion culture. *Cytotechnology* 22, 65–78.
18. Bonarius, H.P.J. et al. (1995) Determination of the respiration quotient in mammalian cell culture in bicarbonate buffered media. *Biotechnology and Bioengineering* 45, 524–535.
19. Frahm, B. et al. (2002) Determination of dissolved CO_2 concentration and CO_2 production rate of mammalian cell suspension culture based on off-gas measurement. *Journal of Biotechnology* 99, 133–148.
20. Madsen, B. (2017) Efficient operation of the HyPerforma 5:1 single-use bioreactor at low working volume, Thermo Fisher Scientific.
21. Madsen, B. et al. (2018) Continuous processing performance enhancements for perfusion applications in 50L to 500L single-use bioreactors: a technical comparison of performance charactreization, cell culture & scale-up modeling. *La Vague* 56, 25–28.

Find out more at **thermofisher.com/sub**

ThermoFisher SCIENTIFIC